



HAL
open science

Modal testing and finite element modelling of a reduced-sized tyre for rolling contact investigation

Yuan-Fang Zhang, Julien Cesbron, Michel Berengier, Hai Ping Yin

► **To cite this version:**

Yuan-Fang Zhang, Julien Cesbron, Michel Berengier, Hai Ping Yin. Modal testing and finite element modelling of a reduced-sized tyre for rolling contact investigation. Euronoise 2015, May 2015, MAASTRICHT, Netherlands. pp.1001-1006. hal-01471765

HAL Id: hal-01471765

<https://hal.science/hal-01471765>

Submitted on 20 Feb 2017

HAL is a multi-disciplinary open access archive for the deposit and dissemination of scientific research documents, whether they are published or not. The documents may come from teaching and research institutions in France or abroad, or from public or private research centers.

L'archive ouverte pluridisciplinaire **HAL**, est destinée au dépôt et à la diffusion de documents scientifiques de niveau recherche, publiés ou non, émanant des établissements d'enseignement et de recherche français ou étrangers, des laboratoires publics ou privés.



Modal testing and finite element modelling of a reduced-sized tyre for rolling contact investigation

Yuan-Fang Zhang, Julien Cesbron and Michel Bérangier

IFSTTAR, AME, LAE, LUNAM Université, Route de Bouaye, CS4, 44344 Bouguenais, France.

Hai-Ping Yin

Université Paris-Est, Laboratoire Navier (UMR 8205), CNRS, ENPC, IFSTTAR, 77455 Marne-La-Vallée, France.

Summary

One of the main contributors to the generation of tyre/road noise is the vibrational mechanism. The understanding of the latter requires both numerical modelling of the tyre/road contact problem under rolling conditions and experimental validation. The use of a go-kart tyre presents advantages in comparison with a standard tyre due to its simpler structure for modelling and its reduced size that facilitates experimental studies in laboratory. Modal testing has first been performed on such a tyre for different inflation pressures to extract modal parameters (frequencies and damping ratios). The modal frequencies are stated to rise accordingly with the inflation pressure. Then, a finite element (FE) vibrational tyre model has been built and adjusted to reproduce similar vibrational characteristics as those obtained from measurements for each tyre inflation pressure investigated. Once validated, the FE model is to be used to simulate the dynamic behaviour of a tyre rolling over a single road asperity for further investigation of the dynamic tyre/road contact problem.

PACS no. 43.40.+s, 43.50.+y

1. Introduction

People are getting more exposed to road traffic noise in urban areas over the last decades [1]. Tyre/road noise is a major contributor to this environmental issue. In particular, for passenger cars rolling at over 50 km/h, it dominates among all the road noise sources [2].

The vibrational mechanisms being an important source of the rolling noise, a better understanding of the role played by the dynamic tyre/road contact is required. Based on classical theories in contact mechanics, many studies have been carried out on the static tyre/road contact problem [3, 4, 5, 6, 7, 8, 9, 10]. Nevertheless, the dynamic contact problem has only been modelled under simplifying assumptions and little investigated through experiments. To examine the dynamic contact laws, a cylindrical test rig has been designed at the IFSTTAR to simulate the road surface on which a tyre will be rolling. A go-kart tyre, due to its reduced size and consequently

its reduced mass, will be easier to manipulate in laboratory and will have less inertial effects during rotations, relative to a standard tyre. Moreover, the latter, composed of multiple layers of different materials, will present more difficulties in modelling [4], hence the choice of using a go-kart tyre on the test rig.

Prior to configuring the test rig for dynamic contact measurements, it is preferable to study the problem through numerical simulations. This paper presents how experimental modal testing results were used to adjust a finite element go-kart tyre model.

2. Description of the go-kart tyre

The go-kart tyre used in this work was a slick commercial tyre from the manufacturer Duro. The tyre code indicating its size was 10-4.50-5 as explained in Figure 1 and corresponded to 114/55R5 in the ISO Metric sizing system. Compared with the car tyres having a size of 205/55R16 used in another modal analysis [11], the go-kart tyre was approximately 40% large in diameter and 56% in width. The tyre tread was composed of a thin rubber layer, the carcass

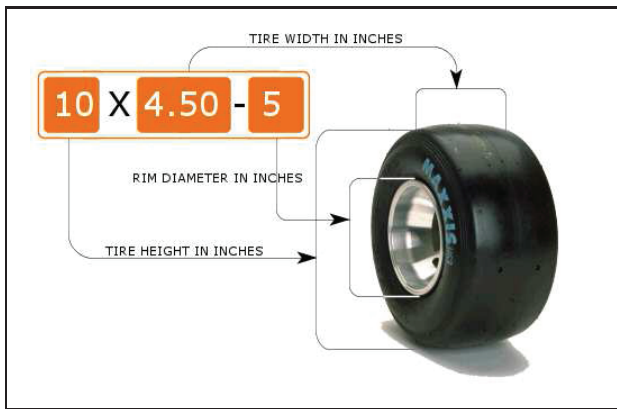


Figure 1: Dimensions of the go-kart tyre. Source: http://www.kartpartsdepot.com/Go_Kart_Wheels_s/1850.htm.

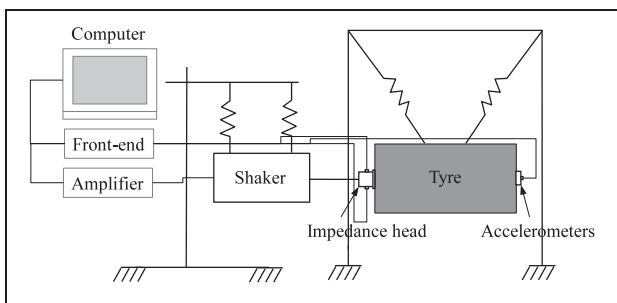


Figure 2: Schema of the experimental set-up for modal testing.

had two rubber coated nylon layers and the bead was reinforced by steel wires. The maximal inflation pressure was 3.9 bars.

3. Experimental modal testing

Modal tests with a classical SIMO (Single-Input Multiple-Output) approach were decided to be performed for 3 different tyre inflation pressures, respectively 0, 1 and 2 bars. The experimental set-up shown in Figure 2 was similar to that used in [11]. All the transducers were connected to a data acquisition front-end from which the data was sent into a software dedicated to modal analysis. To achieve a relatively complete and reliable exploration of the geometrical influences of the tyre on the modal parameters, measurements were carried out at points all around the tyre, spanning from the central rolling band to the sidewalls. The measurement points were marked on the outer contours of 48 cross sections, evenly spaced in the circumferential direction, on each of which 5 equidistantly aligned points were symmetrically placed on both sides about the median point, leading to a total of 528 measurement points.

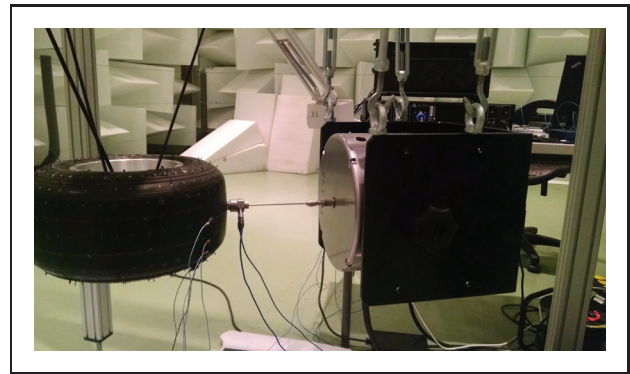


Figure 3: Shaker attached to the suspended tyre.

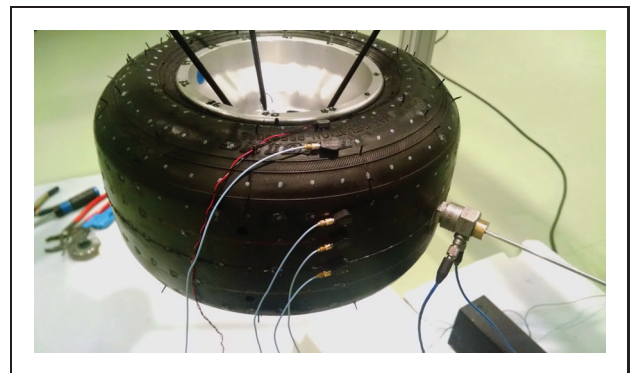


Figure 4: Impedance head and accelerometers mounted onto the suspended tyre.

The cross-sections were numbered from 0 to 47 with the median point of the cross-section number 0 being the drive point, onto which a square aluminium plate of edge length 1 cm was attached. An impedance head was screwed onto the mounting plate. It measured the input force and the output acceleration at the drive point, thus the direct frequency response. The tyre, inflated to the desired pressure, was then horizontally suspended. A shaker was connected to the impedance head by a stinger to exercise a radial excitation force on the tyre, as shown in Figure 3. Figure 4 demonstrates how 5 lightweight single-axis accelerometers were repeatedly mounted each time onto a set of points on the upper or lower part of a cross-section with petro-wax, allowing a temporary and quickly removable adhesion.

To start a measurement, a random signal swept between 0 and 6000 Hz should be generated by the acquisition software and then increased by an amplifier to drive the shaker. Once stabilized, the input force and the direct and transfer output accelerations served to calculate the complex acceleration FRFs (Frequency Response Functions) $H_1(\omega)$ and $H_2(\omega)$ as well as the coherence function $C_{FA}(\omega)$. The acceleration being, in very basic terms, the ratio of the out-

put acceleration signal $A(\omega)$ to the input force signal $F(\omega)$, both in the frequency domain, the two estimates for the FRF $H_1(\omega)$ and $H_2(\omega)$ are defined as follows [12]:

$$H_1(\omega) = \frac{S_{FA}(\omega)}{S_{FF}(\omega)}, \quad (1)$$

$$H_2(\omega) = \frac{S_{AA}(\omega)}{S_{AF}(\omega)}, \quad (2)$$

where $\omega = 2\pi f$ is the angular frequency, $S_{AF}(\omega)$ and $S_{FA}(\omega)$ the cross power spectral density of the input and output signals, $S_{FF}(\omega)$ the power spectral density of the input signal $F(\omega)$ and $S_{AA}(\omega)$ the power spectral density of the output signal $A(\omega)$, all in the frequency domain. The coherence $C_{FA}(\omega)$, i.e. the ratio between $H_1(\omega)$ and $H_2(\omega)$ (Equation 3), whose value is situated between 0 and 1, helps verify the linear link between the drive point and the transfer points. Ideally, the two estimates should be identical, thus the coherence should be 1.

$$C_{FA}(\omega) = \frac{S_{FA}(\omega)S_{AF}(\omega)}{S_{AA}(\omega)S_{FF}(\omega)}, \quad (3)$$

All of the 528 measurement points were investigated for the tyre inflation pressure of 1 bar. The coherence value remained very close to 1 in most of the cases, especially under 3000 Hz, suggesting that using either $H_1(\omega)$ or $H_2(\omega)$ for modal parameter extraction was appropriate. The magnitudes and the phase angles of the complex FRFs $H_1(\omega)$ were plotted for validations of geometrical symmetries. This was first done for the symmetry about the median line around the tyre. The curves proved to be coherent and therefore allowed us to proceed to check the symmetry of measurement results about the excitation direction which also turned out to be true. These two symmetries implied that the measurements for 0 and 2 bars needed only to be performed on a quarter of the tyre.

The measurement results were then imported into the software PULSE Reflex Modal Analysis. The geometry of the quarter of the tyre was built and the FRFs were attributed to the associated point coordinates. The global RFP (Rational Fraction Polynomial) method was chosen to extract modal frequencies and damping ratios from the imaginary part of the complex FRFs [12, 13]. In this method, the complex frequency response in the frequency domain $H(\omega)$ expressed as:

$$H(\omega) = \sum_{k=1}^N \frac{A_k}{\omega_k^2 - \omega^2 + 2i\omega\omega_k\zeta_k}, \quad (4)$$

where N is the number of modes composing the FRF, A_k the k th complex modal constant, ω_k the k th natural frequency and ζ_k the k th modal damping ratio, is alternatively formulated as a rational fraction, i.e. a ratio of two polynomials:

$$H(\omega) = \frac{\sum_{k=0}^{2N-1} a_k(i\omega)^k}{\sum_{k=0}^{2N} b_k(i\omega)^k}, \quad (5)$$

where a_k and b_k are the polynomial coefficients. The coefficients are identified by minimizing the error e_f between the calculated FRF and the measured one $\tilde{H}(\omega_f)$ for each of the measured frequencies ω_f :

$$e_f = \sum_{k=0}^{2m-1} a_k(i\omega_f)^k - \tilde{H}(\omega_f) \sum_{k=0}^{2m} b_k(i\omega_f)^k, \quad (6)$$

where m is the mode order selected for analysis, and the subscript f indicates variables related to measurements. In fact, the global curve-fitting approach in this method can be done in a frequency band chosen to include a certain number of modes. In Figure 5, the measured FRF and the CMIF (Complex Mode Indicator Function) are displayed respectively in red and blue for the inflation pressure of 1 bar. The CMIF was used for preliminary quality checks of the measured data. The curve-fitting frequency range was chosen to be from 280 to 1200 Hz to include the few modes that are identifiable from visual inspection, since peak magnitudes are found at natural frequencies in the imaginary part of accelerance [12, 13]. Figure 5 gives the stability diagram and depicts each natural frequency and the corresponding number of iterations out of 80 at which the stability criterion was fulfilled. Based on the extracted modal parameters, a synthesized FRF was plotted for each measurement point for comparison with experimentation.

Experimental manipulations, tyre geometrical non-uniformity, numerical inaccuracy and other factors could cause erroneous results of the modal parameter extraction, hence the validation step. The main technique used was the AutoMAC meaning Modal Assurance Criteria by looking at the correlation of a set of modes with themselves. Figure 6 displays the off-diagonal correlation between each mode pair for the inflation pressure of 1 bar. The higher the mode order is, the more likely the mode is correlated with other ones. To determine which modes were to be eliminated, several factors needed to be considered: aberrant damping ratio; strong correlations with other modes; clearly false results from visual inspections of the FRFs; correlation degradation of

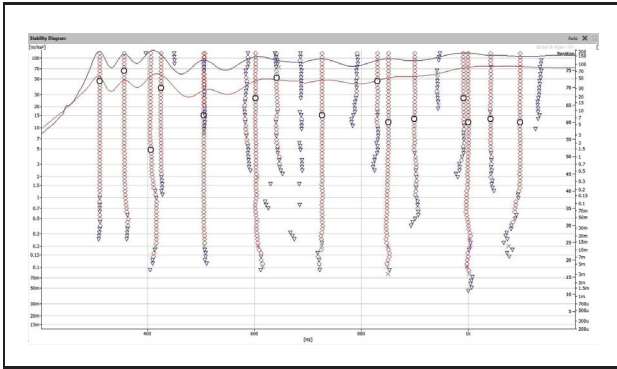


Figure 5: Stability diagram for the tyre inflation pressure of 1 bar.



Figure 6: AutoMAC matrix for the tyre inflation pressure of 1 bar.

Table I: Extracted modal parameters from the measurements for the tyre inflation pressure of 1 bar.

Mode	1	2	3	4	5	6	7	8
$f(\text{Hz})$	310	357	416	505	602	726	850	1000
$\zeta(\%)$	4.9	5.4	4.6	6.2	5.9	5.6	5.8	5.3

the synthesized FRFs with the measured ones.

The frequencies and damping ratios of the retained eigenmodes for the inflation pressure of 1 bar are shown in Table I. The damping ratios are relatively homogeneous. It can be seen from Figure 7 that the modal frequency increases with the tyre inflation pressure at low frequencies.

Figures 8 and 9 represent the magnitude and the phase angle of the directly measured and the synthesized accelerance FRFs respectively at the drive point and at a point making an angle of 90° with the drive point about the tyre axle. The synthesized FRFs correlate well the experimental curves over the curve-fitting frequency range (280 to 1200 Hz).

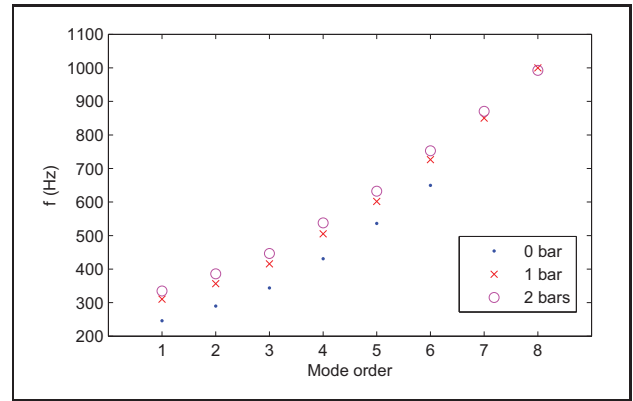


Figure 7: Modal frequencies for tyre inflation pressures of 0, 1 and 2 bars.

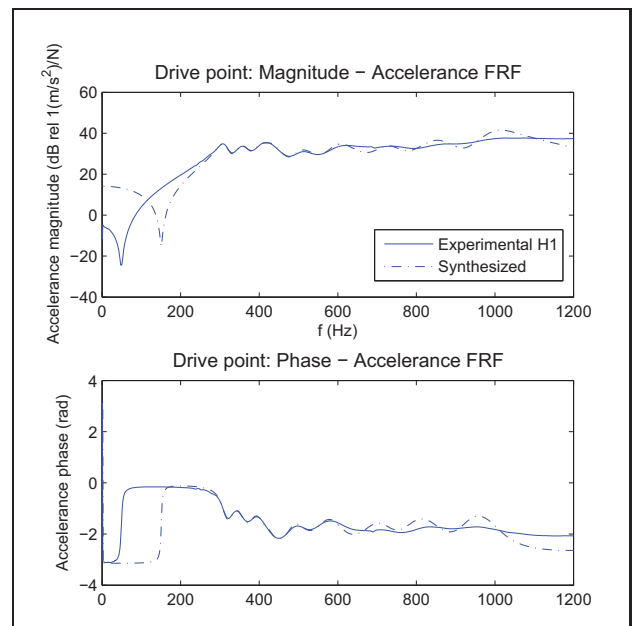


Figure 8: Accelerance FRFs at the drive point for the tyre inflation pressure of 1 bar.

4. Numerical simulation

An FE (Finite Element) model was constructed using Abaqus software for the unloaded tyre on which a numerical frequency response analysis was carried out respectively for the three tyre inflation pressures: 0, 1 and 2 bars. On the one hand, the experimental and the numerical modal analysis results could be mutually validated with the calculated natural frequencies tuned to fit the measured ones; on the other hand, the numerical model could be used for further analyses on the tyre/road rolling contact problem.

The geometry was constructed in three steps as shown in Table II. To take the pressurization of the

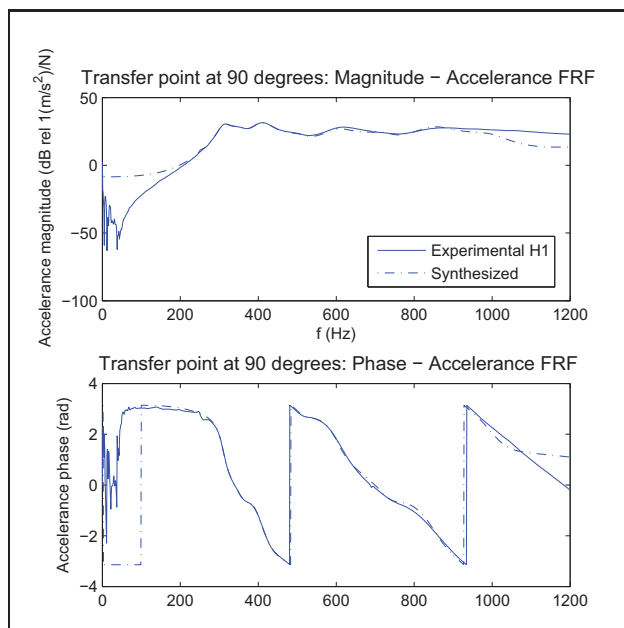





Figure 9: Accelerance FRFs at a transfer point at 90 degrees for the tyre inflation pressure of 1 bar.

Table II: Geometry construction using symmetric results transfer.

Axisymmetric	Partial 3D	Full 3D
		

tyre into account, a distributed load corresponding to the tyre inflation pressure was applied onto the inner side of the tyre. First, an axisymmetric model representing a half cross-section was built and meshed; second, the geometrical deformations of the tyre under pressurization were transferred into a partial three-dimensional model by revolving the axisymmetrical model about the tyre axle to form a half of the tyre; third, the results were transferred into a full three-dimensional model by reflecting the geometry about the tyre's median plane [14]. The structure of the tyre's half cross-section was simplified as a single layer of rubber, considered as an elastic material. Its density was defined as being equal to 1100 kg/m^3 , the Young's modulus 112 MPa and the Poisson's ratio 0.48 . The connection between the rim and the part of the tyre on which the rim was mounted was defined as a rigid body constraint. The movements of the nodes and elements in the median plane was limited within the plane due to the reflection symmetry.

Table III: Extracted modal frequencies from the FE model for the tyre inflation pressure of 1 bar.

Mode	1	2	3	4	5	6	7	8
$f(\text{Hz})$	310	355	419	502	605	729	871	1031

The natural frequencies between 0 and 750 Hz were extracted for the full 3D model with the Lanczos eigensolver [14]. More modes were identified than experimentally, since only circumferential modes with mode order $m = 2$ to 9 were detected through measurements. The modal frequencies are listed in Table III. When comparing them with the experimentally obtained frequency values presented in Table I, a fairly positive correlation can be observed. At the same frequency, two different modes having the same mode shape with a phase shift appear due to the axisymmetry of the tyre model, as stated in [11] and [12].

The next step was to perform a mode-based SSD (Steady-State Dynamic) analysis of the tyre model. A unit force was applied at the drive point node as the input excitation force. Thus, according to the definition of the accelerance, the radial output accelerations at an investigated point gave directly the accelerance FRF. Abaqus allows the option to specify the modes to be considered in this analysis from the aforementioned frequency extraction step and to attribute a modal damping value to each mode number. Compared with Figures 8 and 9, Figures 10 and 11 represent, in addition, the numerically calculated accelerance FRFs at the drive point and the transfer point at 90° obtained by including only the modes at the frequencies in Table III. The correlation is strong from 280 Hz up to 800 Hz.

5. CONCLUSIONS

An experimental modal analysis was first carried out on a go-kart tyre for the tyre inflation pressures of 0, 1 and 2 bars. A classical single-input multiple-output modal testing technique with shaker was used. The rational fraction polynomial method was employed to extract the eigenfrequencies under 1200 Hz and the corresponding damping ratios. The frequencies rise accordingly with the tyre inflation pressure. The synthesized accelerance frequency response functions at the drive point and a transfer point correlate strongly with the measured ones over the curve-fitting frequency range.

Then, a finite element tyre model was constructed in 3D by exploiting tyre's symmetries. The same circumferential modes were extracted as experimentally.

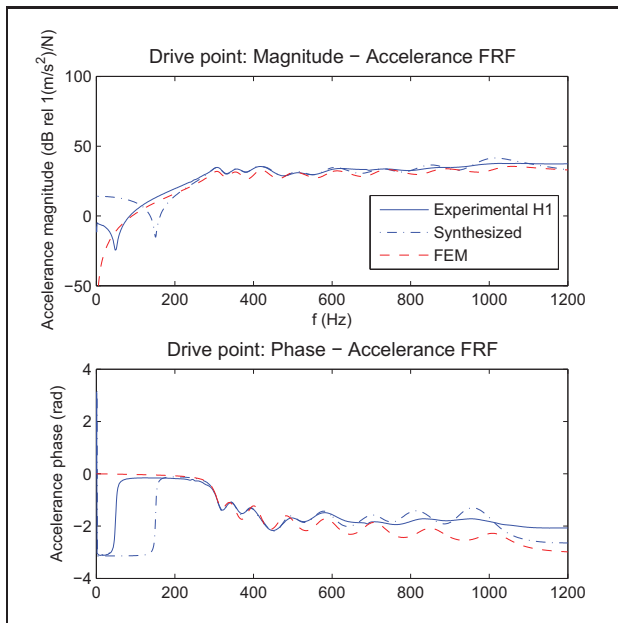


Figure 10: Accelerance FRFs at the drive point for the tyre inflation pressure of 1 bar in comparison with a 3D FE model.

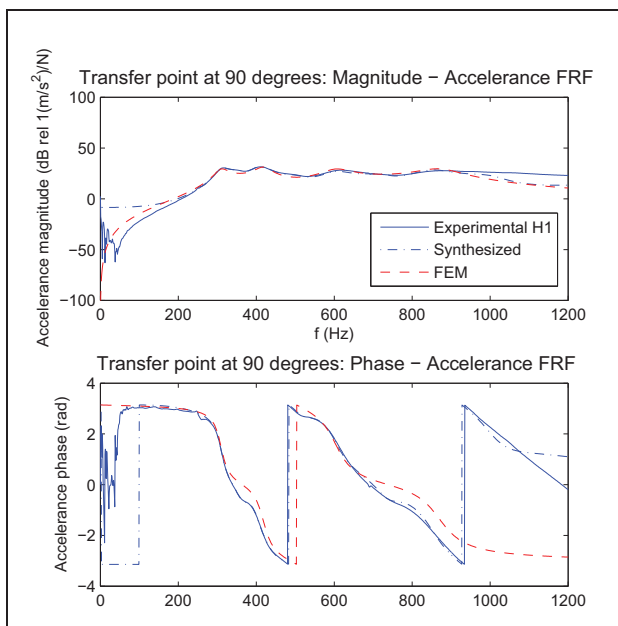


Figure 11: Accelerance FRFs at a transfer point at 90 degrees for the tyre inflation pressure of 1 bar in comparison with a 3D FE model.

The modal frequency values are fairly close. A mode-based steady-state dynamic analysis performed for the detected circumferential modes yielded directly the complex accelerances at the drive point and the transfer point, since the input excitation force was unity. The numerically calculated FRFs correlate satisfyingly with the experimental ones between 280

and 800 Hz.

This unloaded tyre model, simulating correctly the modal properties, up to 800 Hz, will next be used to analyse the rolling contact problem of a loaded tyre. The modes are expected to bifurcate as the axisymmetry will no longer exist for the rolling tyre. The simulation results will provide predictive insights into the configurations and adjustments of a test rig onto which the go-kart tyre will be mounted for measurements of dynamic contact forces.

Acknowledgement

This work was co-funded by the Pays de la Loire region in France and IFSTTAR.

References

- [1] European Environment Agency (EEA): Noise in Europe 2014.
- [2] U. Sandberg: Tyre/road Noise - Myths and Realities. Proc. INTER-NOISE 2001.
- [3] W. Kropp: Ein Modell zur Beschreibung des Rollgeräusches eines unprofilierten Gürtelreifens auf rauher Straßoberfläche. VDI-Verl., 1992.
- [4] K. Larsson, W. Kropp: A high-frequency three-dimensional tyre model based on two coupled elastic layers. JSV 253 (2002) 889-908.
- [5] F. Wullens, W. Kropp: A Three-Dimensional Contact Model for Tyre/Road Interaction in Rolling Conditions. Acta Acustica united with Acustica 90 (2004) 702-711.
- [6] P. Andersson, W. Kropp: Time domain contact model for tyre/road interaction including nonlinear contact stiffness due to small-scale roughness. JSV 318 (2008) 296-312.
- [7] P. Klein, J. F. Hamet: Road texture and rolling noise: an envelopment procedure for tire-road contact. 2004.
- [8] J. Cesbron, H.-P. Yin, F. Anfosso-Lédée, D. Duhamel, D. Le Houédec, Z. Feng: Numerical and experimental study of multi-contact on an elastic half-space. IJMS 51 (2009) 33-40.
- [9] R. Meftah, D. Duhamel, J. Cesbron, H.-P. Yin: Une méthode rapide pour calculer un produit de convolution avec une fonction de Green : application au problème de contact dynamique. Proc. CSMA 2011.
- [10] G. Dubois, J. Cesbron, H.-P. Yin, F. Anfosso-Lédée: Numerical evaluation of tyre/road contact pressures using a multi-asperity approach. IJMS 54 (2012), 84-94.
- [11] P. Kindt, P. Sas, W. Desmet, F. De Coninck: Experimental modal analysis of radial tires under different boundary conditions. Proc. ICSV 2013.
- [12] D. J. Ewins: Modal testing: theory, practice, and application. Research Studies Press, 2000.
- [13] P. L. Gatti, V. Ferrari: Applied Structural and Mechanical Vibrations: Theory, methods and measuring instrumentation. Taylor & Francis, 2003.
- [14] Dassault Systèmes Simulia Corp., Providence, RI, USA: ABAQUS Documentation, 2012.